Combined Effect of Chain Length and Phase State on Adhesion/Friction Behavior of Self-Assembled Monolayers

Dae Ho Lee, Taebyoung Oh, and Kilwon Cho*

Department of Chemical Engineering, School of Environmental Science and Engineering, Polymer Research Institute, Pohang University of Science and Technology, Pohang 790-784, South Korea

Received: March 10, 2005; In Final Form: April 13, 2005

The combined effects of phase state and chain length on the adhesion and friction behavior of self-assembled monolayers (SAMs) are demonstrated using atomic force microscopy (AFM). The phase state of *n*-alkyltrichlorosilane monolayers of varying chain length (C-8, C-12, and C-18) was controlled by adjusting the preparation temperature. The adhesion forces and friction coefficients were observed to increase dramatically around the phase-transition temperature of each monolayer. The phase state effect was more prominent for the longer chain SAMs, which is attributed to the larger deformation volume associated with disordered monolayers. The adhesion/friction diagram for chain length effect with a wide range of phase states is successfully presented. This study reveals that the chain length effect on adhesion/friction can be correctly evaluated by examining the phase-state dependence of adhesion/friction behind the chain length effect.

Introduction

Nanoadhesion and nanofriction have become important issues with regard to miniaturized devices such as thin-film transistors, MEMS devices, and bio-interfaces.[1−7] Adhesion is associated with the intermolecular forces (physical/chemical) that occur between the interfacial atoms or molecules of two materials at the mutual point of contact. These intermolecular forces constitute the origin of the surface or interfacial energy of the two materials.[8] Adhesion is also associated with the mechanical properties of adherends or adhesives, where the energy is consumed through viscoelastic or plastic deformation during the detachment process. Thus, adhesion energy can be described in terms of the intrinsic work of adhesion (W) and the dissipation energy factor Φ.[9−14]

Friction, on the other hand, is composed of two processes, namely normal loading and lateral sliding. Here, the intermolecular forces act as a barrier toward sliding and viscoelastic or plastic deformation during both processes.[15−24] In the case where a substrate is penetrated by a probe, the energy dissipation during lateral sliding can be significant. Therefore, like adhesion, friction is also a phenomenon produced from a mutual contribution of intermolecular force and energy dissipation.

Through recent investigations on the adhesion/friction behavior of single molecular layers [e.g., self-assembled monolayers (SAMs)], it has been recognized that the Φ contribution can be significant even at the nanoscale. Adhesion/friction strength (force or energy) is known to be highly dependent on several physical factors such as chain length, packing density, and phase state (order/disorder).[21,24−36]

The effects of monolayer chain length often lead to inconsistent results. For a probe (e.g., an AFM tip) modified with a suitable monolayer, it was reported that the adhesion/friction forces increase with increasing chain length due to the more effective interdigitation that occurs between the surface monolayer and the modified probe.[26,27] However, in the case where an inorganic probe (e.g., a Si_3N_4 tip) was used,[21,24,28−34] higher adhesion/friction forces were observed with decreasing chain length, since the shorter chains invariably form disordered monolayers with loosely packed structures. Here, the decreasing chain length facilitates molecular contact between the inorganic probe and the monolayer due to the increased ease of surface penetration into the loosely packed monolayer, resulting in an increase in contact area. However, different adhesion/friction behaviors have been observed for monolayers of *n*-alkyltrichlorosilanes and alkanethiols[35] and even for monolayers of the same chain length and surface functionality.

It is possible that the chain length effect on adhesion/friction is also dependent on other physical conditions such as phase state and packing density. As stated above, the involvement of these properties has already been considered. However, it has not been possible to demonstrate the effects of chain length and phase state on adhesion/friction behavior experimentally.

Work relating to the phase state effect on adhesion/friction behavior has previously been conducted using a range of different materials, all with varying chain lengths.[21−36] More recently however, our group[37] has simplified this study by concentrating on the phase-transition nature of monolayers formed from just *n*-alkyltrichlorosilanes. In this case, a fixed chain length ($n = 18$, C-18) monolayer was used, and the effects of phase state on the changes in adhesion behavior were investigated. In the current work, we build upon the results obtained in the previous investigation by considering the effects of different monolayer chain lengths on other physical properties such as phase state. Although the effect of packing density should also be considered,[37] the results obtained by adjusting just the chain length and phase state alone are expected to provide a useful insight into methods to control the adhesion/friction behavior at the nanoscale.

Experimental Section

Materials. Octadecyltrichlorosilane [$CH_3(CH_2)_{17}SiCl_3$, C-18], dodecyltrichlorosilane [$CH_3(CH_2)_{11}SiCl_3$, C-12], octyltrichlo-

* To whom all correspondence should be addressed. E-mail: kwcho@postech.ac.kr.

10.1021/jp051232t CCC: $30.25
Published on Web 05/14/2005

rosilane [$CH_3(CH_2)_7SiCl_3$, C-8], and anhydrous toluene (Aldrich) were used as received. All alkylsilanes and anhydrous toluene were stored in a desiccator prior to use. P-type Si(100) wafers (Shinetsu) were cleaned in piranha solution (70% vol H_2SO_4 + 30% vol H_2O_2) for 30 min at 100 °C, then washed with copious amounts of distilled water, and stored under vacuum prior to use.

Monolayer Preparation. Vacuum-dried reaction flasks were charged with anhydrous toluene and cleaned Si wafers under argon. The flasks were then placed in a temperature-controlled bath and allowed to stand for 30 min to ensure thermal equilibrium. Alkyltrichlorosilanes were then added to the flask containing toluene (10 mM concentration of alkyltrichlorosilane solution) and left to self-assemble on the wafers for 2 h under argon. The silicon wafers were removed from solution, rinsed repeatedly with toluene and ethanol, and then baked in an oven at 120 °C for 20 min. After baking, the substrates were cleaned by ultrasonication in toluene and rinsed thoroughly with toluene and ethanol, followed by vacuum-drying prior to use.

Surface Characterization. Monolayer thickness was determined using an ellipsometer (M-2000V, J. A. Woollam Co. Inc.), whereas the chain conformation was investigated by analyzing the absorption spectra obtained from a Fourier transform infrared spectrometer (FT-IR, Bruker IFS 66v), using p-polarized light with an incident angle of 80°. Surface wettability was determined by measuring the contact angle formed between a probe liquid (distilled water or hexadecane) and the monolayer surface using a contact angle meter (Krüss BSA 10). The monolayer surface topography was examined using atomic force microscopy (AFM) (Autoprobe CP, Park Scientific Instruments). AFM images were obtained in contact mode, using silicon nitride cantilevers with a force constant of 0.1 N/m, and a scan rate of 1.0 Hz.

Adhesion Force Measurements. Adhesion forces were measured between the AFM tip (Si_3N_4, spring constant: 0.1 N/m, given by manufacturer) and SAMs by recording the cantilever deflection in the force-displacement (attraction-retraction) curves. AFM experiments were performed at a relative humidity controlled within the range of 25−35% under a nitrogen atmosphere in order to minimize the effect of capillary force. The magnitude of the pull-off jump in the retraction portion of the force-displacement curve corresponds to the adhesion force. The tip scanning speed was maintained at 1 μm/s, with an applied force of 1 nN. To minimize the variability of the tip shape, the same tip was used throughout the investigation. Reliable pull-off force measurements were obtained by averaging 10 data points per sample by recording the fore-displacement curves at different locations on the surface.

Friction Force Measurements. Friction measurements were performed using an Autoprobe CP scanning probe microscope (Park Scientific Instruments), equipped with Ultralevers (spring constant: 0.4 N/m, given by manufacturer). Friction forces were measured by recording traces of cantilever lateral diffraction (friction loops) over scan areas of 1 μm × 1 μm with a sliding velocity of 1 μm/s. Friction forces were averaged for more than 20 data points per sample at different locations on the monolayer surface. For each friction loop, the difference in the friction signal (voltage) between the forward and reverse scans was converted to friction force by applying Hooke's law. The lateral spring constant, k_{lat}, (∼205 N/m) was estimated using the method reported by Noy and co-workers.[38] All friction measurements were performed at a relative humidity controlled within the range of 25−35%, under a nitrogen atmosphere.

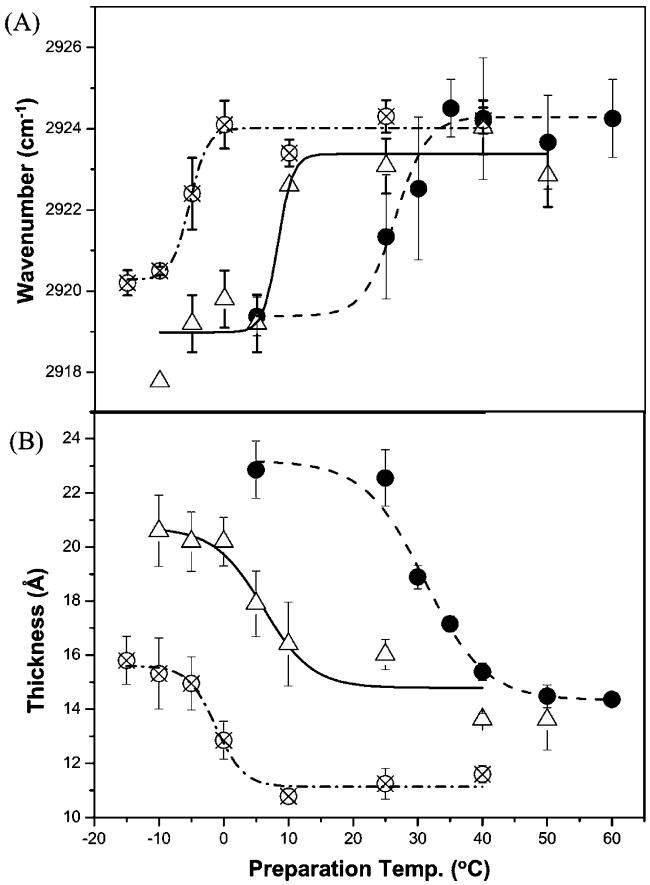

Figure 1. Peak positions of $-CH_2-$ asymmetric vibration obtained using FT-IR (A) and thickness obtained using ellipsometry (B) of C-18 (●), C-12 (△), and C-8 (⊗) monolayers with respect to preparation temperatures.

Results and Discussion

A. Structure of SAMs. Characteristic IR peaks resulting from the methylene ($-CH_2$) stretching vibrations (ca. 2920 cm^{-1}) of well-ordered SAMs were observed for monolayers prepared below their critical temperatures (30 °C for C-18, 5 °C for C-12, and −5 °C for C-8). These characteristic peaks exhibit an upward shift as the preparation temperature is increased (Figure 1A), indicating that the ordered, mainly trans conformation chain structures, transform into disordered structures with increasing gauche-defects.[39,40] The monolayer thicknesses determined by ellipsometry (Figure 1B) reveal a sharp decrease around the corresponding transition temperatures. This result coincides with the IR observations, implying that a reduction in the monolayer thickness corresponds with an increase in structural disorder. From these results, the observed transition temperatures: ∼30 °C for C-18, ∼5 °C for C-12, and ∼ −5 °C for C-8 were found to be in good agreement with previously reported values.[39−42]

Octadecyltrichlorosilane on oxidized silicon is known to have a tilt angle of 10∼20° from the surface normal.[46−48] Wasserman et al.[46a] have shown that thickness of silane-based monolayers has a linear relationship with the chain length, and they conclude that tilting of the chains is small (14 ± 18°) irrespective of chain length. Vallant et al.[46b] have found a slight increase (5∼15°) in the tilt angle upon chain length reduction and attributed the change in tilt angle to the increased disorder upon decreasing chain length, which was evidenced by the position of $-CH_2$ stretching peaks of IR spectroscopy. However, our result indicates that the monolayers prepared below each T_c are all in the well-ordered state (FT-IR, Figure 1A), and that they have

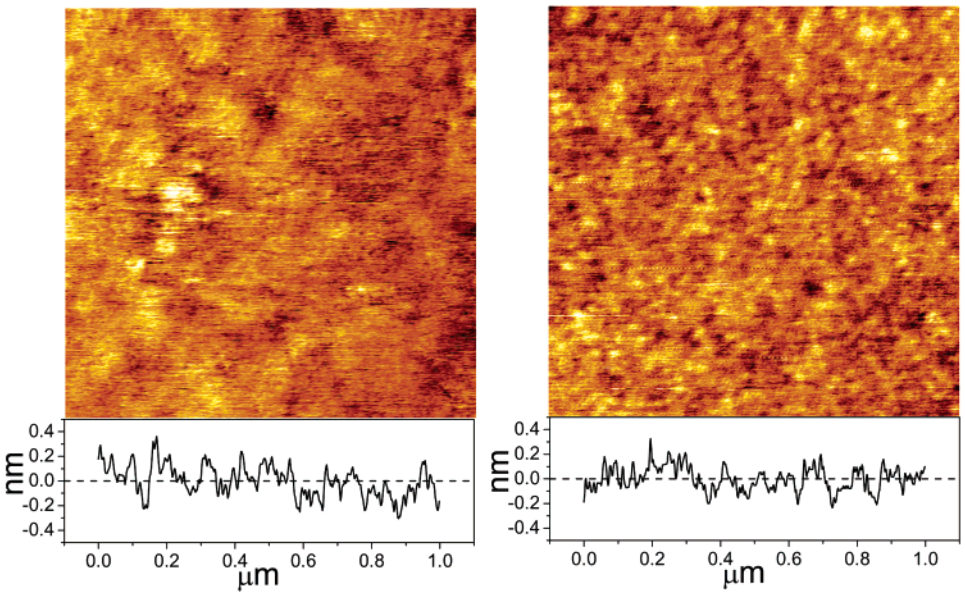

Figure 2. AFM images of ordered (left) and disordered (right) C-12 monolayers (rms roughness is ~ 1 Å irrespective of chain length and phase state). Similar images (with similar surface roughness) were obtained for C-18 and C-8 monolayers (not shown).

TABLE 1: Surface Wettabilities of Monolayers Using Hexadecane as a Probe Liquid[a]

C-18		C-12		C-8	
prep. temp °C)	contact angle (°)	prep. temp (°C)	contact angle (°)	prep. temp (°C)	contact angle (°)
5	40	−10	40	−15	40
25	40	−5	40	−10	40
30	40	0	40	−5	39
35	38	5	38	0	38
40	38	10	38	10	38
50	38	25	38	25	38
60	38	40	38	40	38
		50	37		

[a] Error bar of each data is ~±1 °C. Water contact angles were varied from ~106 °C for ordered monolayers to ~102 °C for disordered monolayers for three kinds of monolayers (C-18, C-12, C-8 monolayers), which are similar with those in previous publication.[37]

small tilt angles based on the calculation from the results of ellipsometry (Figure 1B). It should be noted that determination of the tilt angle from the effective thickness is somewhat indirect and not very precise, since the change of the effective thickness with the tilt angle (θ) goes as $\cos(\theta)$ and, therefore, is not very sensitive at small angles.[48] Although the tilt angle was not precisely determined in this work, it is speculated that three kinds of monolayers in the ordered state do not have any significant difference in their molecular structure, and if any, only minor contribution to other physical properties such as adhesion or friction is expected which will be discussed in the next section.

The surface morphologies of the monolayers were observed to be both homogeneous and smooth (roughness ~1 Å), irrespective of the monolayer chain length and conformation, as confirmed by AFM (Figure 2). The corresponding surface wettabilities (obtained from contact angle measurements) were essentially the same for all monolayer surfaces (Table 1), where slight decreases (1~2°) in angle for the disordered monolayers are thought to result from the exposure of $-CH_2$ toward the outermost surface. From these results, it can be concluded that the silicon substrates possess a complete monolayer coverage in all cases, and that the molecular density of the prepared monolayer is not sufficient to alter the surface properties.

B. Adhesion Force. The adhesion forces associated with the prepared monolayers (C-8, C-12, and C-18) were investigated using AFM. Figure 3 shows the results obtained from the AFM force-displacement curves (Si_3N_4 tip) for monolayers of various chain length and phase state. Striking differences in the adhesion forces, together with simultaneous conformational changes, were observed around the transition temperature for each monolayer. As discussed previously,[37] the observed increase in adhesion force for disordered monolayers is attributed to the increased mobility of the disordered monolayer chains. Therefore, as the monolayer structure becomes disordered, and a weaker mechanical resistance is realized,[43−45] the AFM probe is able to penetrate deeper into the monolayer, resulting in a concomitant increase in contact area during the tip-attraction process. These increases in contact area and monolayer chain mobility can also result in greater deformation of the disordered monolayer during the tip-retraction process. Consequently, as the preparation temperature is raised (increasing disorder), the contact area increases allowing greater deformation, and a concomitant increase in adhesion force.

Considering the adhesion force around 40 °C, it is apparent that monolayers with longer chains give rise to higher adhesion forces when disordered. In other words, the phase state effect becomes more prominent as the chain length increases. This result is due to the differences in the deformation behavior, since the surface energies for each monolayer are essentially the same. It is therefore likely that the increased adhesion force observed for disordered monolayers of long chains is due to an increase in the deformation volume, as shown in Figure 5. However, one should also consider whether the relative disorder and relative packing density are similar for disordered monolayers of varying chain length.

The relative packing density of a monolayer can be inferred from its change in thickness. As seen in Figure 1, the percentage decrease in thickness of the disordered monolayers is typically 35%. This result implies that, if the packing densities of ordered monolayers are similar and assumed to be 100%, then those of the corresponding disordered monolayers will be approximately 65%, irrespective of chain length. The relative disorder of a monolayer can be estimated from the position of the asymmetric stretching vibration in the corresponding FT-IR spectrum. As

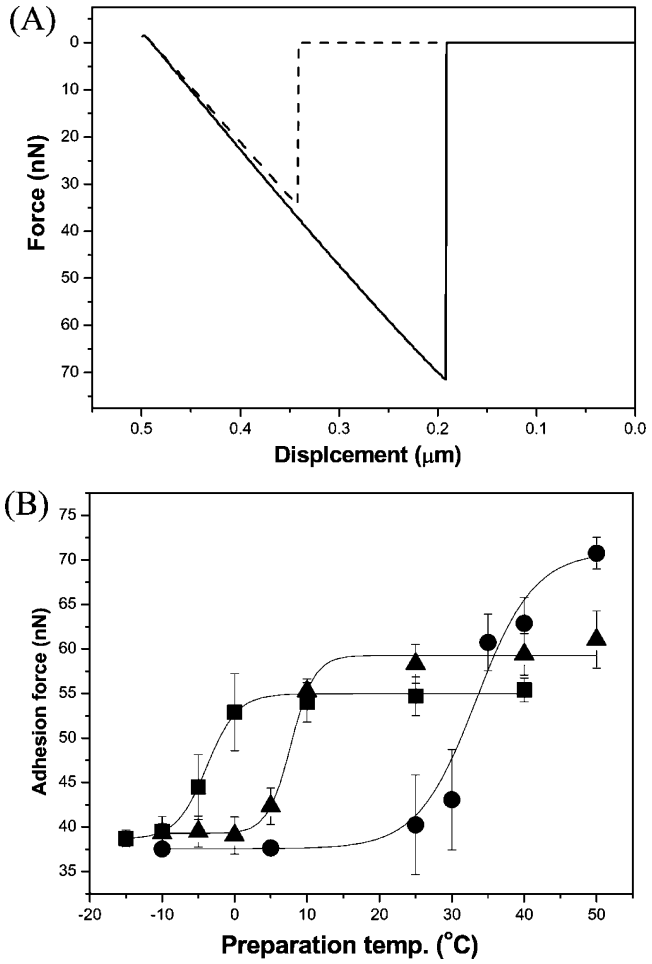

Figure 3. Adhesion forces of SAMs. (A) Representative force-displacement curves for monolayers with different phase state obtained using AFM (C-18 monolayer, ordered (upper) and disordered (lower)). (B) Adhesion (pull-off) forces between AFM tip and monolayers of various phase state and chain length (C-18 (●), C-12 (▲), and C-8 (■) monolayers).

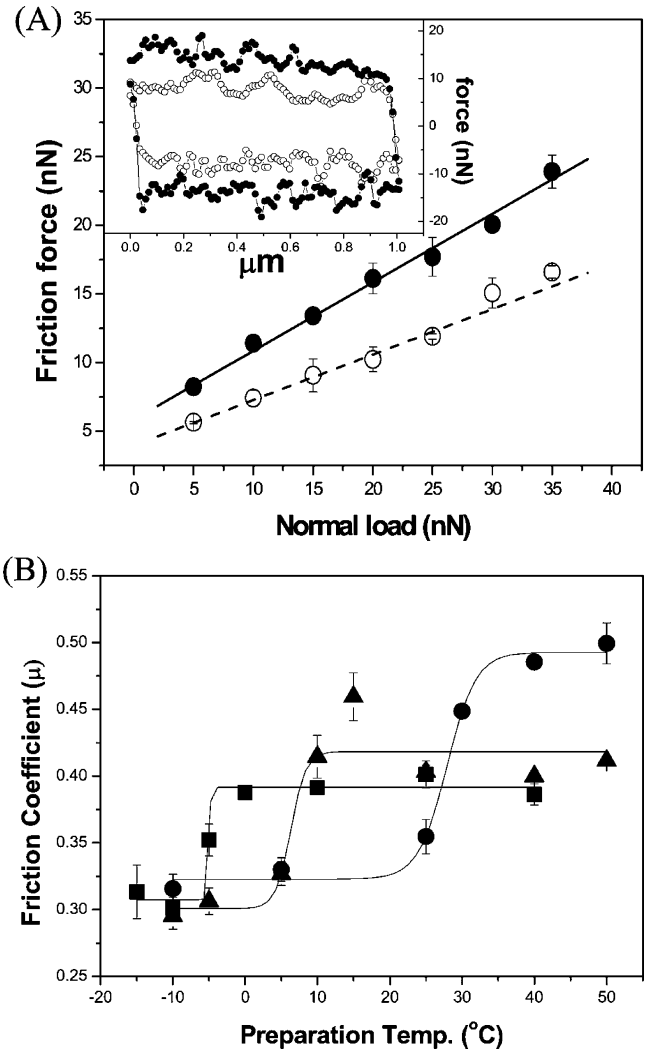

Figure 4. Friction forces of SAMs. (A) Representative normal load-friction force plots with different phase state obtained using AFM (C-18 monolayer, ordered (lower) and disordered (upper)). Representative friction loops for ordered (open symbol) and disordered (filled sympol) monolayers (under normal load of 20 nN) are inserted in the graph. (B) Friction coefficients between AFM tip and monolayers of various phase states and chain lengths (C-18 (●), C-12 (▲), and C-8 (■) monolayers).

shown in Figure 1A, the $-CH_2-$ peak position is essentially the same for all disordered monolayers, implying that the relative disorder is similar, irrespective of chain length. From these results, it can be suggested that the deformation volume is primarily responsible for the increased adhesion forces associated with the long chain, disordered monolayers.

As for the chain length effect, it should be noted that the adhesion forces are only different above the corresponding T_c (disordered structure), while adhesion forces below T_c (ordered structure) are almost constant, irrespective of chain length. If the adhesion behaviors of monolayers with fixed chain length and various phase states are compared,[37] it can be found only that the disordered monolayers are *relatively* more deformable than the ordered monolayers. However, it is difficult to ascertain whether ordered monolayers are deformable or not, and if they are, then their degree of relative deformability is difficult to establish from experimental conditions. Here, the results show that the adhesion behavior of ordered monolayers is not substantially affected by their chain length, which strongly suggests that the deformation of ordered monolayers is minimized under the current experimental conditions.

C. Friction Force. As seen in Figure 4, the frictional forces are linearly proportional to the normal loads, with a slope which can be defined as a friction coefficient μ (= friction force/normal load).[12] Further, the frictional forces show a quite different normal load-dependence with regards to the phase state of the monolayers. Although the relationship between the normal loads and frictional forces is unlikely to follow Amonton's law over the wide range of normal loads,[12,13,16,17] it does provide a convenient means to compare the friction coefficients between the different phase states of the monolayer. Moreover, this relationship is also deemed to represent physical conditions such as monolayer deformation during tip sliding on the SAM surface. Figure 4B shows the friction coefficients with regards to the monolayer chain length and phase state.

As in adhesion, surface energy and molecular deformation are key factors that need to be considered when determining frictional values. The observed friction coefficients for the (C-8, C-12, and C-18) monolayers reveal a similar trend to those obtained for the adhesion forces. This is likely to result from the deformation behavior of the monolayers, since the observed surface energies show minimal effect. For the disordered monolayers, the increased contact area afforded by tip penetration is not only responsible for the increased adhesion force, but it also provides a convenient route for the dissipation of energy during sliding. Ordered monolayers on the other hand,

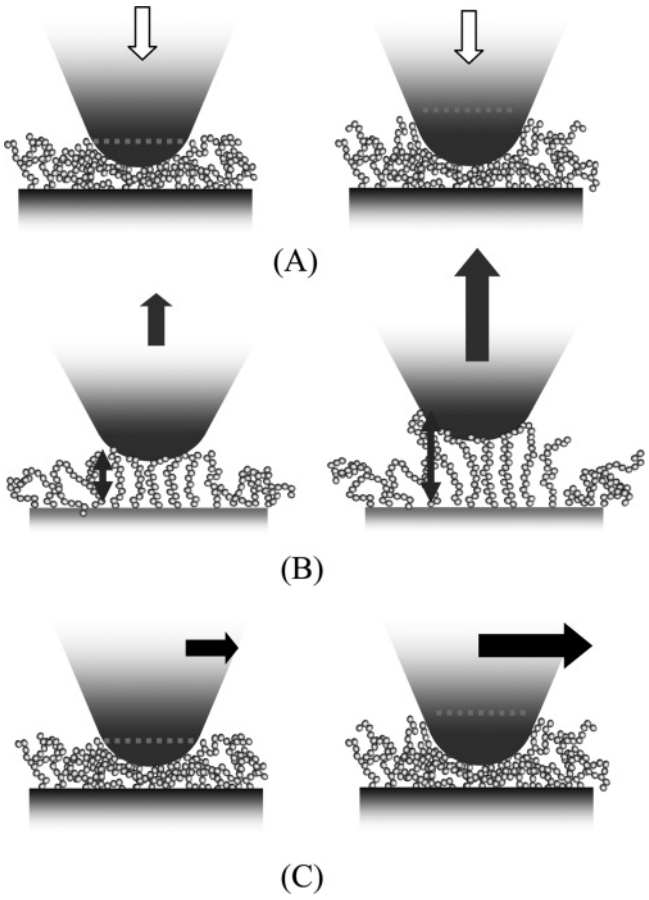

Figure 5. Schematic illustrating monolayer deformation of short (left) and long chain (right) disordered monolayers. (A) Penetration of AFM tip into disordered monolayer causes an increase in contact area. This results in greater monolayer deformation during pull-off (B) and tip-sliding (C) on monolayer surfaces, which is more prominent for longer chain disordered monolayers due to the increased deformation volume.

are not expected to restrict tip sliding, since the energy dissipation afforded by monolayer deformation is minimal.

The occurrence of possible interactions between the silicon substrate and the AFM tip, via long-range van der Waals forces, are not apparent in this study, since higher friction and adhesion are expected for the short chain, disordered monolayers, where the distance between the tip and the bare substrate is essentially closer. Thus, the occurrence of higher adhesion forces and friction coefficients for long chain, disordered monolayers, effectively rules out the possibility of any tip-wafer interactions, suggesting that the deformation volume provides a major contribution to both increased adhesion and friction values in these monolayers.

It should be emphasized here that the experimental results concerning the effects of chain length could be easily misinterpreted. For example, if monolayers of varying chain length are prepared at room temperature and the adhesion/friction behavior compared, it is possible to conclude that the adhesion/friction force is greater for the shorter chain lengths. Moreover, it may also be concluded that additional differences in the physical states of the monolayers are responsible for the "unexpected" outcome in which the C-12 monolayer yields higher adhesion/friction forces than the short-chained C-8 monolayer. Indeed, slight changes in the surrounding conditions (such as ambient temperature) could quite easily lead to a misinterpretation of the results. Consequently, it is imperative to consider the total phase changes (from ordered to disordered) to compare the effects of chain length. Therefore, of the three (C-18, C-12, and C-8) monolayers prepared at room temperature, the C-18 monolayer exhibits the lowest adhesion/frictional force on account of its ordered structure, which is not subject to deformation by the AFM tip. Moreover, the adhesion/frictional forces are higher for the C-12 monolayer than for the C-8 monolayer since, despite both being in the disordered state, the C-12 monolayer has a potentially larger deformation volume than the C-8 monolayer.

Analysis of friction loop can supply more detailed information on friction behavior, usually by analyzing the atomic-scale stick-slip behavior of the substrate, as reviewed by Carpick and Salmeron.[15] However, in our experimental condition, we observed no significant difference in the friction-loop pattern for monolayers of different phase state or chain length. We only observed the similar friction profile during lateral scan (inset in Figure 4A), however with different average friction forces and normal-load dependence, which were dramatically affected by the phase state and chain length of monolayers.

Conclusions

The effects of chain length on the adhesion and friction behavior of SAMs have been studied with respect to phase state. The adhesion/friction forces for disordered monolayers revealed dramatic increases in all cases. Increases in both adhesion and friction for disordered monolayers became more prominent with increasing chain length, which is attributed to the increase in deformation volume. In contrast, the adhesion/friction forces for ordered monolayers were small and effectively constant, irrespective of chain length. This suggests that ordered monolayers are not deformable under the current experimental conditions. The phase state-adhesion/friction diagram obtained for various monolayer chain lengths demonstrates how molecular structure and adhesion/friction behavior are clearly related at the nanoscale.

Acknowledgment. The authors thank the Ministry of Science and Technology of Korea (National Research Laboratory Program), the Ministry of Education of Korea (BK21 Program), the Advanced Environmental Biotechnology Research Center at Pohang University of Science and Technology, and the Regional Technology Innovation Program (grant No. RTI04-01-04) of the Ministry of Commerce, Industry, and Energy for their financial support.

References and Notes

(1) Stutzmann, N.; Friend, R. H.; Sirringhaus, H. *Science* **2003**, *299*, 1881.
(2) Kagan, C. R.; Mitzi, D. B.; Dimitrakopoulos, C. D.; *Science* **2000**, *286*, 945.
(3) Srinivasan, U.; Houston, M. R.; Howe, R. T.; Maboudian, R. *J. Microelectromech. Syst.* **1998**, *7*, 252.
(4) López, G. P.; Albers, M. W.; Schreiber, S. L.; Carroll, R.; Peratta, E.; Whitesides, G. M. *J. Am. Chem. Soc.* **1993**, *115*, 5877.
(5) Willner, I.; Schlittner, A.; Doron, A.; Joselevich, E. *Langmuir* **1999**, *15*, 2766.
(6) Knoll, W.; Zizlsperger, M.; Liebermann, T.; Arnold, S.; Badia, A.; Liley, M.; Piscevic, D.; Schmitt, F.-J. *Colloids Surf. A* **2000**, *161*, 115.
(7) Chapman, R. G.; Ostuni, E.; Liang, M. N.; Meluleni, G.; Kim, E.; Yan, L.; Pier, G.; Warren, H. S.; Whitesides, G. M. *Langmuir* **2001**, *17*, 1225.
(8) Dupré, Théorie Méchanique de la Chaleur; Gauthier-Villars; Paris, 1869; p 369.
(9) A. J. Kinloch, *Adhesion and adhesives*; Chapman & Hall: New York, 1987; p 270.
(10) Ghatak, A.; Vorvolakos, K.; She, H.; Malotky, D. L.; Chaudhury, M. K. *J. Phys. Chem. B* **2000**, *104*, 4018.
(11) Ruths, M.; Granick, S. *Langmuir* **1998**, *14*, 1804.
(12) Ruths, M.; Granick, S. *J. Phys. Chem. B.* **1998**, *102*, 6056.
(13) Barthel, E.; Roux, S. *Langmuir* **2000**, *16*, 8134.

(14) Bistac, S. *J. Colloid Interface Sci.* **1999**, *219*, 210.
(15) Carpick, R. W.; Salmeron, M. *Chem. Rev.* **1997**, *97*, 1163.
(16) Singer, I. L. *J. Vac. Sci. Technol. A* **1994**, *12*, 2605.
(17) Berman, A.; Drummond, C.; Israelachvili, J. *Tribology Lett.* **1998**, *4*, 95.
(18) Tsukruk, V. V.; Bliznyuk, V. N. *Langmuir* **1998**, *14*, 446.
(19) Clear, S. C.; Nealy, P. F.; *J. Colloid Interface Sci.* **1999**, *213*, 238.
(20) Vorvolakos, K.; Chaudhury, M. K. *Langmuir* **2003**, *19*, 6778.
(21) McDermott, M. T.; Green, J−B. D.; Porter, M. D. *Langmuir* **1997**, *13*, 2504.
(22) Subbotin, A.; Brinke, G. T.; Kulichikhin, V. G.; Hadziioannou, G. *J. Chem. Phys.* **1998**, *109*, 827.
(23) Carpick, R. W.; Agrait, N.; Ogletree, D. F.; Salmeron, M. *J. Vac. Sci. Technol. B* **1996**, *14*, 1289.
(24) Leggett, G. J. *Anal. Chim. Acta* **2003**, *479*, 17.
(25) Chen, Y. L.; Helm, C. A.; Israelachvili, J. N. *J. Phys. Chem.* **1991**, *95*, 10736.
(26) van der Vegte, E. W.; Subbotin, A.; Hadziioannou, G. *Langmuir* **2000**, *16*, 3249.
(27) Nakagawa, T.; Ogawa, K.; Kurumizawa, T. *J. Vac. Sci. Technol. B* **1994**, *12*, 2215.
(28) Xiao, X.; Hu, J.; Charych, D. H.; Salmeron, M. *Langmuir* **1996**, *12*, 235.
(29) Koleske, D. D.; Barger, W. R.; Lee, G. U.; Colton, R. J. *Mater. Res. Soc. Symp.* **1997**, *464*, 377.
(30) Kiely, J. D.; Houston, J. E.; Mulder, J. A.; Hsung, R. P.; Zhu, X.-Y. *Tribology Lett.* **1999**, *7*, 103.
(31) Bar, G. *Langmuir* **1997**, *13*, 373.
(32) Clear, S. C.; Nealy, P. F. *J. Chem. Phys.* **2001**, *14*, 2802.
(33) Wong, S.; Takano, H.; Porter, M. D. *Anal. Chem.* **1998**, *70*, 5209.
(34) Liu, Y.; Evans, E. F. *Langmuir* **1996**, *12*, 1235.
(35) Lio, A.; Charych, D. H.; Salmeron, M. *J. Phys. Chem. B* **1997**, *101*, 3800.
(36) Chaudhury, M. K.; Owen, M. J. *J. Phys. Chem.* **1993**, *97*, 5722.
(37) (a) Lee, D. H.; Kim, D. H.; Oh, T.; Cho, K. *Langmuir* **2004**, *20*, 8124. (b) Cho, J. H.; Lee, D. H.; Shin, H. S.; Pattanayek, S. K.; Ryu, C. Y.; Cho, K.; *Langmuir* **2004**, *20*, 11499.
(38) Noy, A.; Frisbie, C. D.; Rozsnyai, L. F.; Wrighton, M. S.; Lieber, C. M. *J. Am. Chem. Soc.* **1995**, *117*, 7943.
(39) (a) Iimura, K.; Nakajima, Y.; Kato, T. *Thin Solid Films* **2000**, *379*, 230.
(40) Rye, R. R. *Langmuir* **1997**, *13*, 2588.
(41) Brzoska, J. B.; Azouz, I. B.; Rondelez, F. *Langmuir* **1994**, *10*, 4367.
(42) Parikh, A. N.; Allara, D. L.; Azouz, I. B.; Rondelez, F. *J. Phys. Chem.* **1944**, *98*, 7577.
(43) Chen, Y. L.; Helm, C. A.; Israelachvili, J. N. *Langmuir* **1993**, *7*, 2694.
(44) Leng, Y.; Jiang, S. *J. Chem. Phys.* **2000**, *113*, 8800.
(45) Quon, R. A.; Ulman, A.; Vanderlick, T. K. *Langmuir* **2000**, *16*, 3797.
(46) (a) Wasserman, S. R.; Tao, Y.; Whitesides, G. M. *Langmuir* **1989**, *5*, 1074. (b) Wasserman, S. R.; Whitesides, G. M.; Tidswell, I. M.; Ocko, B. M.; Pershan, P. S.; Axe, J. D. *J. Am. Chem. Soc.* **1989**, *111*, 5852. (c) Tidswell, I. M.; Rabedeau, T. A.; Pershan, P. S.; Kosowsky, S. D.; Folkers, J. P.; Whitesides, G. M. *J. Chem. Phys.* **1991**, *95*, 2854.
(47) (a) Vallant, T.; Kattner, J.; Brunner, H.; Mayer, U.; Hoffmann, H. *Langmuir* **1999**, *15*, 5339. (b) Heid, S.; Effenberger, F.; Bierbaum, K.; Grunze, M. *Langmuir* **1996**, *12*, 2118. (c) Harder, P.; Bierbaum, K.; Woll, C.; Grunze, M.; Heid, S.; Effenberger, F. *Langmuir* **1995**, *11*, 512.
(48) Schreiber, F. *Prog. Surf. Sci.* **2000**, *65*, 151.